Hydrophobic Clusters Regulate Surface Hydration Dynamics of *Bacillus subtilis* Lipase A

Afnan M Jaufer,[a] [b] *Adam Bouhadana,*[a] *and Gail E Fanucci**[a] [b]

[a] Department of Chemistry, University of Florida, P.O. Box 117200, Gainesville, Florida 32611, United States

[b] George and Josephine Butler Polymer Research Laboratory, University of Florida, Gainesville, FL 32611, United States.

KEYWORDS. Lipase A, EPR, Spin-Labeling, Hydration, ODNP Relaxometry. Diffusive water

ABSTRACT

The surface hydration diffusivity of *Bacillus subtilis* Lipase A (BSLA) has been characterized by low-field Overhauser dynamic nuclear polarization (ODNP) relaxometry using a series of spin labeled constructs. Sites for spin-label incorporation were previously designed via an atomistic computational approach that screened for surface exposure, reflective of the surface hydration comparable to other proteins studied by this method, as well as minimal impact on protein function, dynamics, and structure of BSLA by excluding any surface site that participated in greater than 30 percent occupancy of a hydrogen bonding network within BSLA. Experimental ODNP relaxometry coupling factor results verify overall surface hydration behavior for these BSLA spin-labeled sites similar to other globular proteins. Here, by plotting the ODNP parameters of relative diffusive water versus the relative bound water, we introduce an effective "phase-space" analysis, which provides a facile visual comparison of ODNP parameters of various biomolecular systems studied to date. We find notable differences when comparing BSLA to other systems, as well as when comparing different clusters on the surface of BSLA. Specifically, we find a grouping of sites that corresponds to the spin-label surface location within the two main hydrophobic core clusters of the branched aliphatic amino acids isoleucine, leucine and valine cores observed in the BSLA crystal structure. The results imply that hydrophobic clustering may dictate local surface hydration properties, perhaps through modulation of protein conformations and samplings of the unfolded states, providing insights for how dynamics of the hydration shell is coupled to protein motion and fluctuations.

INTRODUCTION

Lipases have several biotechnologically interesting characteristics.[1-7] The extracellular lipolytic activity of *B. subtilis* was first observed in 1979 by Kennedy and Lennarz.[8] However, intensive molecular research did not start over a decade later in 1992, with the cloning and sequencing of a lipase gene, lipA (lipaseA),[9] followed by recombinant expression, purification and functional and structural characterizations.[10] *B. subtilis* lipases are the smallest lipases known with molecular masses of ~19.5 kDa, and are representative of lipases that have no lid domain.[11, 12] Because of this, they do not show any activation in the presence of an oil water interface; the catalytic serine (Serine-77) is located on the surface of the protein and is freely accessible to the solvent.[11-13] Recently, it has recently been proposed from molecular dynamic simulations that loop 1- within *B. subtilis* lipase A (BSLA) can act as a "lid" and induce reorientation at an interface as a form of enzymatic activation.[13, 14] Given its unique utility because of its status as a lid-less lipase,[11, 12, 15, 16] many studies have been conducted with the objective towards understanding its mechanism of function[13] as well as engineering BSLA to have enhanced thermostability, chemostability, substrate specificity, and solubility.[17-37] Of particular interest is understanding modifications, such as amino acid substitutions and polymer conjugation, that allow BSLA to function in organic solvents,[30] ionic liquids,[24, 25, 32] and as solvent-free protein biofluids. [34, 36, 37]

In summary, much work has been conducted in the quest to push the functional limits of BSLA as an enzyme for biotechnological applications. Many of these studies touch on effectively manipulating the intra-molecular forces and overall structure of the protein, while others rely on modifying the surface of the protein in some form to bring about a desired effect. The focus of characterizing the underlying mechanisms of these changes has demonstrated how protein

structure and intra-molecular interactions impact stability and function. Yet, the fundamental characterization of the hydration of BSLA is known only from approaches to enhance solubility within organic solvents.[30, 33]

Here, to further elucidate the local hydration dynamics around the surface of BSLA, Overhauser dynamic nuclear polarization (ODNP) relaxometry is used to characterize the local hydration within the 5-15 Å sphere around each spin-label on the surface of a wild-type-like R1 BSLA construct (Figure 1, Table S1). The results gained show a narrow dispersion in hydration behavior for diffusive waters and bound water behavior that bunch together according to the location of the reporters within two main hydrophobic clusters of the branched aliphatic amino acids isoleucine, leucine, and valine (ILV) cores observed in the BSLA crystal structure. Thus, these results set a reference for future comparative studies of other BSLA constructs and modified (bioconjugate or tethered) systems. Additionally, the results imply that hydrophobic clustering may dictate local surface hydration properties; perhaps through modulation of protein conformations and samplings of the unfolded states.[38-48]

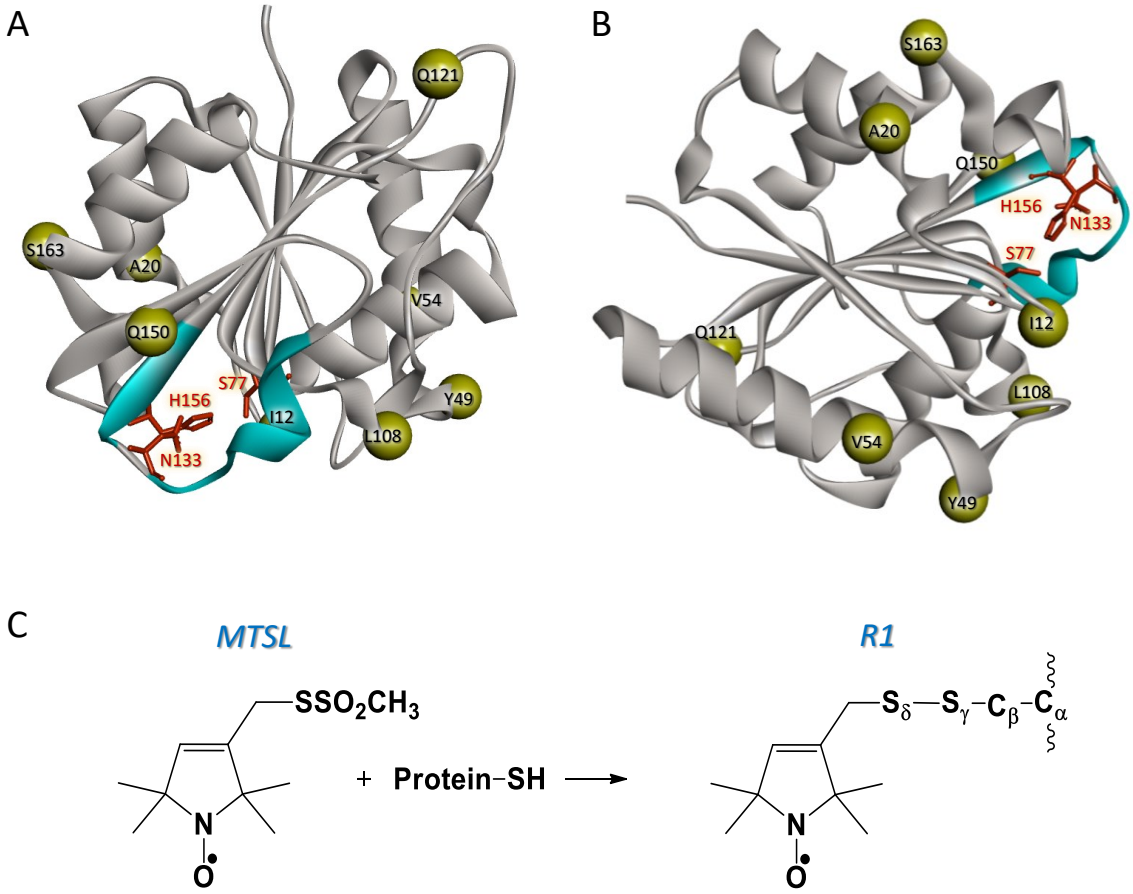

Figure 1. Two different views of spin-labeled sites in BSLA (PDB ID 1ISP) with Cα carbons shown in Van der Waals format displayed in yellow for those sites substituted by cysteine. Catalytic triad, S77-N133-H156, shown in red, with loop 1 (Y129-R142) – a hypothesized amphipathic lid, rendered in cyan. Figure on the left (A) orients BSLA to show the typical alpha beta hydrolase fold, whereas the ribbon diagram on the right (B) shows an alternative orientation of the 8 spin-labeled sites. (C) R1 spin labeling scheme of a cysteine residue.

BACKGROUND FOR ODNP

Low-field ODNP relaxometry is a technique that combines X-band CW-EPR spectroscopy and ^{1}H NMR spectroscopy to probe local water relaxometry surrounding a nitroxide spin label.[49-51] It exploits the unpaired electron of the nitroxide radical to enhance the proton NMR signal of water through polarization transfer via Overhauser cross relaxation.[52, 53] This polarization transfer happens locally from the cysteine substituted spin labeled residue giving hydration dynamic

information within 5-15 Å of the nitroxide radical.[49, 50] The water ^{1}H nuclei signal enhancement is determined by the polarization coupling efficiency (ξ), calculated by the following equation:[50, 53]

$$\xi(coupling\ factor) = \frac{\boldsymbol{k_\sigma}\ (cross\ relaxivity)}{\boldsymbol{k_\rho}\ (self\ relaxivity)} \qquad 1$$

Where k_σ and k_ρ are local cross- and self-relaxivity ($s^{-1}M^{-1}$) scaled for spin probe concentration, respectively. These time dependent variables scale relative to the distance between the spin label electron and the ^{1}H water nuclei within 5-15 Å. These relaxivities reflect the diffusive dynamics of the amount of water within this distance. Equation 2 represents a relationship for ξ, based on the applied force free hard sphere (FFHS)[54] model, demonstrating an analytical form of the spectral density function $J(\omega)$ thus describing a translational dipolar correlation time of local water (τ_c).[50]

$$\boldsymbol{\xi} = \frac{\boldsymbol{6J(\omega_e - \omega_H, \tau_c) - J(\omega_e + \omega_H, \tau_c)}}{\boldsymbol{6J(\omega_e - \omega_H, \tau_c) + 3J(\omega_H, \tau_c) + J(\omega_e + \omega_H, \tau_c)}} \qquad 2$$

Where, Equation 3 shows the form of the is the spectral density function, $JFFSH(w, tc)$,defined by the FFHS model.[54]

$$\boldsymbol{J_{FFHS}(\omega, \tau_C)} = \boldsymbol{(1 + \frac{5\sqrt{2}}{8}(\omega\tau)^{\frac{1}{2}} + \frac{\omega\tau}{4})/(1 + (2\omega\tau)^{\frac{1}{2}} + (2\omega\tau) + \frac{\sqrt{2}}{3}(\omega\tau)^{\frac{3}{2}} + \frac{16}{81}(\omega\tau)^2 + \frac{4\sqrt{2}}{81}(\omega\tau)^{\frac{5}{2}} + \frac{(\omega\tau)^3}{81})} \qquad 3$$

ω_e and ω_H represent the proton and electron Larmor frequencies in radian/sec, respectively. At X – band frequencies and electron lamor frequencies, relative with the standard use of a nitroxide probe, $\omega_e = (2\pi)9.8$ GHz and $\omega_H = (2\pi)14.8$ MHz, making $\omega_e \pm \omega_H$ approximately equal to ω_e. τ_c is interpolated from the experimentally measured coupling factor (Equation 2), assuming the spectral density function given in Equation 3. By using this relationship, it is possible to generate a plot of $\boldsymbol{\xi}$ as a function of $\boldsymbol{\tau_C}$, and mark all the coupling constant values of previous hydration studies (Figure 2). In this manner, ODNP relaxometry has been used to probe different types of

hydration environments.[49, 50, 55-68] In this routine, the solid line in Figure 2 represents the theoretical dependence of ξ on τ_c dictated by Eq. 2 and Eq 3 and the dotted lines represent boundaries of bulk-like(ξ >0.27), surface DNA and polyampholytes (0.153 < ξ ≤0.27), surface globular proteins (0.076< ξ ≤0.153), intermediate (0.043< ξ ≤0.076) and buried (ξ ≤0.043) hydration diffusivity. These demarcations represent a semi-objective classification of water location determined from the myriad of systems encompassing proteins, nucleic acids, polymers and lipid dispersions previously characterized by ODNP by Han and co-workers.[50, 55-57, 61-64, 69]

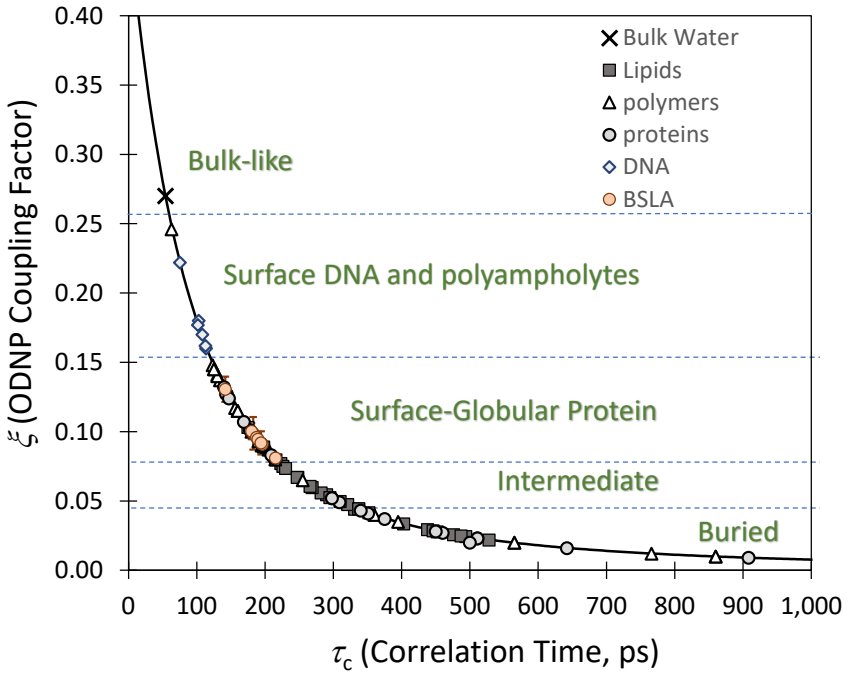

FIGURE 2: Plot of collective literature-based ξ values and their modeled relationship to τ_c [90] for lipid systems (solid squares), proteins (grey circles), DNA (grey diamonds)[55] and synthetic polymers (white triangles).[50, 56, 57, 61-64, 69] Data obtained for R1-BSLA variants are shown as orange circles. Figure modeled after those shown by Han and co-workers.[56] The solid line is the theoretical relationship between the coupling factor and the correlation time determined from the spectral density function with the force free hard sphere model. Dotted lines represent designated water-type areas characterized for systems studied by ODNP.

Han and co-workers have further shown that the ODNP cross-relaxation and self-relaxation parameters can be further analyzed in terms of k_σ and k_{low} that allows for the selection of different regimes of water motion in the analysis of hydration water dynamics.[50, 55, 56, 60, 68] This analysis provides a differentiation of fast diffusing water (DW) on the picosecond timescale (k_σ), and slower diffusing or "bound" water (BW – waters that have rotational correlation times dictated by the macromolecule) on the millisecond-nanosecond timescale (k_{low}).[49, 55, 60] Equation 4 gives the relationship to calculate values of k_{low}.[50]

$$k_{low} = \frac{5}{3}k_\rho - \frac{7}{3}k_\sigma \tag{4}$$

For easy comparison to other systems studied by ODNP relaxometry, a scaled parameter for DW via Equation 5, can be obtained by referencing ODNP relaxometry parameters obtained for sites on a macromolecule to those values obtained for a nitroxide spin-label in bulk water, $k_{\sigma,\,bulk}$.[56]

$$k_{\sigma scaled} = \left(\frac{k_{\sigma,site}}{k_{\sigma,bulk}}\right)^{-1} \tag{5}.$$

Because data for $k_{\sigma,\,bulk} > k_{\sigma,\,site}$ as reported to date in the literature,[68] Eq. 5 is written as an inverse function to give values > 1, and this scaled parameter is referred to within as the relative DW hydration, that scales this parameter to discuss quantitatively a slowing of the surface diffusive water layer or can alternatively be viewed as reflecting on the "enthalpic cost for disrupting and displacing the hydration water that is collectively strengthened by the attractive interactions between the protein surface and the hydrogen-bonds of the local water network" [60] compared to those waters interacting with the nitroxide in water; which is defined as bulk hydration diffusivity. Analogously, k_{low} enhancements, referred to within as relative BW, can be compared to bulk values as defined by Equation 6. [56, 60]

$$k_{low\text{-}enhancement} = \left(\frac{k_{low,site}}{k_{low,bulk}}\right) \quad (6)$$

Note that Eq. 6 is not an inverse with literature reports showing ranges of this value from 0.25 to ~ 3. [68]

MATERIALS AND METHODS

Preparation of Spin-Labeled BSLA.

We recently generated a series of surface spin-labeled BSLA constructs (Figure 1), there are no native cysteines in *B. subtilis* lipase A,[70] and showed these spin-labeled variants retained near wild-type structure, thermal stability, and enzymatic activity.[71] Spin-label sites were chosen to reflect high side-chain mobility, to have high surface accessibility and to be located close to locations of future bioconjugation to surface lysine residues. The results of our studies are intended to elucidate the relationships among sequence, structure, dynamics and bioconjugation in relationship to surface hydration for understanding rational protein engineering of the BSLA surface to achieve specific desirable properties and protein function. Here, wild-type, cysteine substituted variants (I12C, A20C, Y49C, V54C, L108C, Q121C, Q150C, and S163C) of wild-type BSLA sequence (Table S1) within plasmids were transformed into L21(DE3) pLysS competent cells which were then grown in 1 L LB media at 37 °C at 250 rpm until optical density at 600 nm (OD600) was between 0.6 and 0.8. Subsequently the expression of BLSA was induced by 1mM IPTG (isopropylthio-β-galactoside) for 24 hours. Protein was isolated, purified, and spin-labeled via a procedure we modeled after those reported earlier by others,[29, 71, 72] as is described in detail in the Supporting Information. Finally, the spin-labeled samples were verified via mass spectrometry (Table S2) and stored at 20˚C in a buffer of 10 mM Na_2HPO_4 at pH 7.0.

ODNP sample preparation. Approximately *3.5*µl of a given R1-BSLA construct in 10 mM Na_2HPO_4 at pH 7.0 in was drawn into 0.6 mm I.D. x 0.84 mm O.D. Supracil/quartz capillary tubes (Fiber Optic Center; New Bradford, MA), via capillary action. The samples were sealed with a protective layer of Critoseal on the top and bottom. The concentration of WT and spin labeled BSLA constructs were calculated by measuring A_{280nm} value at diluted volumes of each stock solution in triplicate. The theoretical molar extinction coefficient of the enzyme is 24,410 $M^{-1}cm^{-1}$.[35] Spin label concentration was verified by comparing the double integral area of the R1-BSLA EPR spectrum to those from X-band CW EPR spectroscopy of a TEMPO standard curve and was > 90% comparable to A_{280nm} measured protein concentration. Given comparable spin label concentration and > 95% spin labeling efficiency determined through mass spectrometry mass analysis, final protein concentration used for sample preparation and data analysis was determined from TEMPO standard curve, as the MTSL moiety likely increases the theoretical molar extinction coefficient, rendering A_{280nm} values that have a systematically higher value than that determined from UV-VIS measurements. X-band (9.5 GHz) CW-EPR absorption spectra for standard curve, spin-concentration, and verification of sample integrity before and after ODNP, were collected at room temperature using a Bruker E500 spectrometer with a dielectric resonator. Spectra were reported as an average of 16 scans with 120 G sweep width, 0.6 G modulation amplitude, 100 kHz modulation frequency and 2 mW incident microwave power. EPR spectra were baseline corrected and double integral area normalized using Origin software. Each sample was prepared to ~ 200 µM protein concentration. BSLA tended to aggregate at higher concentrations. To achieve a concentration suitable for ODNP measurements, solution parameters utilized in previous NMR studies[29] were employed. We also found that unmodified purified his-tagged BSLA[35] would

precipitate out of solution above 80 μM; hence this motivated our overexpression strategy[71] to follow the inclusion body approached of non-his-tagged BSLA utilized by Kaar and co-workers in their NMR investigations,[29] as our ODNP signal enhancements were low for concentrations < 100 μL.

ODNP Data Collection.

All samples were run using a Bruker dielectric resonator modified with inserted ODNP probe (Bridge12, Inc,) with an X-band/Q-band Bruker E500 EPR spectrometer with a custom-built 2 W 9.8 GHz source similar to the one described by Han and co-workers.[73] The frequency of the microwave source was set to ~9.6 GHz (monitored via a Phase Matrix, Inc. EIP model 28B frequency counter) and determined by the field (~0.35 T) of the central resonance of the EPR spectrum of the nitroxide labelled protein. The rf tuning circuit was tuned to ~14.8 MHz to match the applied magnetic field. Microwave power was monitored by Gigatronics 8541C Universal Power Meter. A Benchtop Techmag spectrometer was utilized for NMR data acquisition. The 90-degree pulse width for the NMR experiment was set at 2 microseconds as determined by nutation experiment. Recycle delays were typically set ~ 20 s to ensure 5-8x the longest T_1. The ^{1}H free induction decay signal and the $T_{1,\,^1H}$ relaxation time for each sample were measured as a function of microwave power from 0 to *~400 mW*. Both the $T_{1,\,^1H}$ *and* $T_{1,0}$ (spin lattice relaxation of the sample without spin label) was measured using inversion recovery pulse sequences. Each enhancement and T_1 experiment pair were performed in triplicate, where each run was performed on a separate sample from the same purification/labeling batch and placed in fully cleaned (0.60 inner-diameter. x 0.84 outer-diameter). capillary tubes. Dried air, regulated to 25°C by passing through a recirculating water bath, flowed past the sample. Data was analyzed via Microsoft Excel,

with the solver add-on used to generate fits for all data from this experiment, as performed previously.[68] ODNP data and analysis are given in the Supporting Information (Figures S9 and S10, Tables S6 and S7) and follow the procedures described previously.[49, 60, 74 68]Final plots for Figures within were generated using either MS Excel, Origin 8.5 and protein image rendering was done via VMD (version 1.9.3) or Biovia Design Studios.

RESULTS AND DISCUSSION

ODNP Data Analysis

Each R1-BSLA sample was subjected to three types of ^{1}H NMR experiments. The first of these is the Overhauser DNP enhancement experiment, which records the ~14.6 MHz ^{1}H NMR signal as a function of applied microwave radiation (~ 9.6 GHz) to saturate the nitroxide spin resonance. Analysis of the enhancement data provides values of $\boldsymbol{k}_\sigma$ (Figure 3). In the enhancement experiment, the first data point is obtained by collecting a ~14.6 MHz ^{1}H NMR signal from the sample with no incident microwave power. Every datapoint succeeding this is collected with a level of irradiated MW power. To minimize heating effects and to help prevent protein aggregation over the course of the experiment, we vary the power of the data collection in a manner where all even numbered attenuations of MW power were collected first, in descending order (32 dB, 30 dB, 28 dB, etc.), with odd numbered attenuations of MW power collected in ascending order (16dB, 18 dB, 20 dB, etc.). Integrals of the ^{1}H NMR signal obtained at different levels of MW power are then processed via Equation 4, where $I(\mathrm{p})$ and $I(0)$ are peak integrals at microwave powers "p" and "$p = 0$" respectively.[49]

$$\boldsymbol{\varepsilon(p) = \frac{I(p) - I(0)}{I(0)}} \quad 4$$

The second type of experiment is a series of ~14.6 MHz ^{1}H NMR T_1 measurements as a function of ~ 9.5 GHz microwave power, $T_1(p)$, that spans the powers utilized in the enhancement series.[49] It has been demonstrated that increased microwave irradiation leads to sample heating, thus requiring T_1 measurements as a function of power.[49, 50] Together, the values of ε(p) are used in combination with longitudinal relaxation time from the $T_1(p)$ experiments to calculate $\boldsymbol{k_\sigma}$. As mentioned by Franck and Pavlova, the $\varepsilon(p)$ can be written as shown in equation 5 and rearranged to give Equation 6. [50]

$$\boldsymbol{\varepsilon(p) = T_1(p) k_\sigma s(p) C_{SL} \left|\frac{\omega_e}{\omega_H}\right|} \quad 5$$

$$\boldsymbol{k_\sigma s(p) = \left(\frac{0.015167}{C_{SL}}\right) \frac{\epsilon(p)}{T_1(p)}} \quad 6$$

Here, T_1(p) is the NMR longitudinal relaxation time—*i.e.,* the time constant for relaxation of the NMR signal to thermal equilibrium, s(p) is the saturation factor (the net electron spin saturation across all three hyperfine transitions of the nitroxide) for a range of microwave powers, p, C_{SL} is the concentration of the spin label, and ω_e and ω_H are the electron and proton Larmor frequencies, respectively.

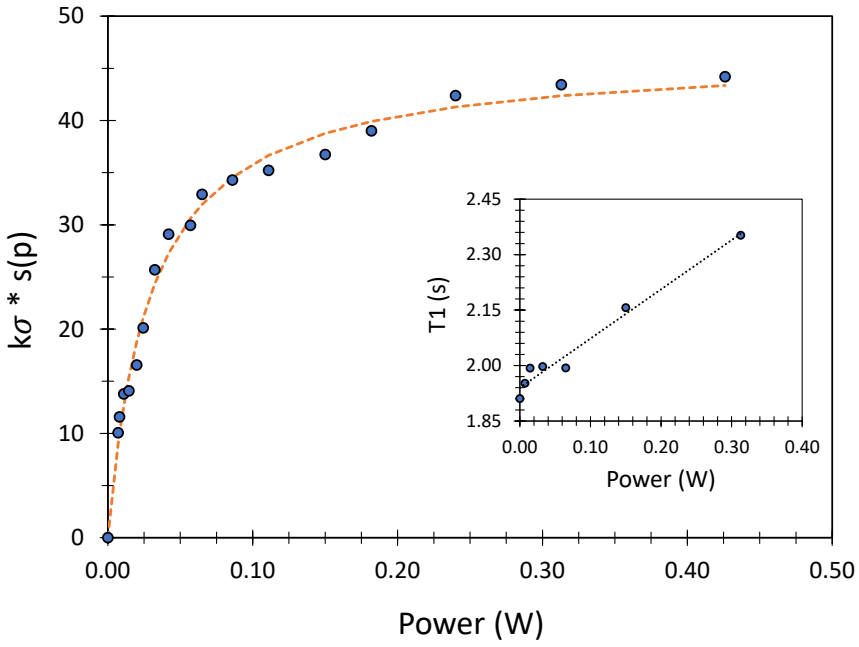

FIGURE 3: Plot of representative R1-BSLA ODNP enhanced ^{1}H NMR signal curve according to Equation 6. Data given here are for Q121R1. Dotted red line shows a fit to the data using Equation 7. Inset shows the corresponding T_1 values determined for samples under the given value of microwave power. Linear regression of the measured T_1(p) was used to provide values in Equation 6. The increase observed in T_1 as a function of applied microwave power indicates sample heating.[49, 50]

Figure 3 show representative ODNP relaxometry enhancement data for BSLA with $T_1(p)$ results shown as an inset. Enhancement and $T_1(p)$ profiles were collected for each R1-BSLA variants in triplicate using fresh protein samples from a given purification of spin-labeled BSLA for each experimental run. All enhancement and $T_1(p)$ curves are given in the Supporting Information (Figures S2-S9). Values for k_σ are obtained from fitting the enhancement curves to the right side of Equation 7.[49]

$$\boldsymbol{k_\sigma s(p) = \frac{k_\sigma s_{max} p}{p_{1/2} + p}} \qquad 7$$

Here, $p_{1/2}$, a parameter that reports the microwave power that achieves half saturation of the electron spin transition, and $k_\sigma s_{max}$ are the fit parameters. It is known that s_{max} is approximately equal to 1 for nitroxides tethered to biological macromolecules,[49, 50] which is the case in our experiments, and hence it is possible to obtain k_σ through the fitting. Table 1 summarizes values of k_σ obtained for all R1-BSLA variants.

Table 1. Summary of ODNP parameters determined for R1-BSLA.

Variant	k_σ ($s^{-1}M^{-1}$)	$(k_\sigma/k_{\sigma bulk})^{-1}$	k_ρ ($s^{-1}M^{-1}$)	k_{low} ($s^{-1}M^{-1}$)	k_{low}/k_{low_bulk}	ξ	τ_c (± 1 ns)	τ_c/τ_{cbulk}
I12R1	41± 5	2.30 ± 0.29	430 ± 50	600 ±100	1.6 ± 0.3	0.09 ± 0.02	182	2.31 ± 0.29
A20R1	38.4 ± 2.2	2.47 ± 0.15	383 ± 25	550 ± 40	1.47 ± 0.19	0.100 ± 0.006	180	2.47 ± 0.15
Y49R1	44.4 ± 1.7	2.13 ± 0.10	460 ± 20	670 ± 30	1.78 ± 0.21	0.096 ± 0.002	187	2.13 ± 0.10
V54R1	37.3 ± 0.8	2.54± 0.08	460 ± 5	680 ± 9	1.81 ± 0.19	0.081 ± 0.002	215	2.54 ± 0.08
L108R1	30.8 ± 1.2	3.07 ± 0.14	340 ± 10	493 ± 14	1.32 ± 0.15	0.091 ± 0.002	195	3.08 ± 0.14
Q121R1	43 ± 3	2.18 ± 0.16	330±20	450 ± 30	1.20 ± 0.15	0.131 ± 0.010	141	2.20± 0.16
Q150R1	33.0 ± 0.2	2.85 ± 0.07	352 ± 17	500 ± 30	1.36 ± 0.16	0.095 ± 0.002	189	2.87 ± 0.07
S163R1	33 ± 3	2.86 ± 0.27	360 ± 40	530 ± 80	1.42± 0.26	0.092 ± 0.018	194	2.9 ± 0.3

The "bulk" values for nitroxide (TEMPO) in water are 94.71 ($s^{-1}M^{-1}$) and 375.1 ($s^{-1}M^{-1}$) for $\boldsymbol{k_\sigma}$ and $\boldsymbol{k_{low}}$ respectively. These values were obtained from previous work by Frank *et al.*[49, 50]

The third type of measurement is an NMR T_1 experiment in the absence of any microwave irradiation to obtain values for $\boldsymbol{k}_\rho$. The T_1 measurements of the spin labelled, and non-spin labelled (WT) protein samples are then used in equation 8 to yield $\boldsymbol{k}_\rho$.[50]

$$k_\rho = \frac{1}{C_{SL}}\left(\frac{1}{T_1} - \frac{1}{T_{1,0}}\right) \quad (8)$$

Where T_1 and $T_{1,0}$ are the T_1 measurements of the spin labelled and non-spin labelled (i.e. WT) samples respectively. Values of k_ρ for R1-BSLA variants are also given in Table 1. Next k_σ and k_ρ values are used to calculate the ODNP coupling parameter ξ according to Eq (1). These calculated values of values of ξ, and their corresponding values of τ_c (via Eq. 2 and Eq. 3) are given in Table 1. Values of the ODNP coupling factors, ξ, for each R1-BSLA variant are given in Table 1 and plotted in Figure 2 in a style consistent with the Han group presentation of X-band ODNP results.[56] Our results for BSLA are plotted in Figure 2 as orange spheres, where each shows surface-like hydration diffusivity of the waters surrounding all of the chosen spin-labelled sites.

The ratio of ξ/ξ_{bulk} (or $\tau_c/\tau_{c,bulk}$), where bulk are the values obtained hydroxy-tempo in bulk water,[49, 50, 56] can be used as a comparative parameter to describe the effective impedance in hydration diffusivity relative to bulk water.[50] Our results indicate the hydration waters on the surface of BSLA are 3-4 times slower than those of bulk water around a spin-label. Additionally, the ODNP results demonstrate that the computational approach to picking surface sites of BSLA[71] resulted in successfully identifying surface-like hydration sites.

Distinguishing Diffusive Versus Bound Water on BSLA

As we described in our recent ODNP studies of an intrinsically disordered protein, IA_3, an analysis of k_σ and k_{low} values normalized to bulk water values plotted against one another provides a graphical "phase space" that disperses the difference in hydration behavior arising from DW versus

BW scaled to bulk.[68] Figure 4 shows the phase space representing the heterogeneity of the hydration environment of the BSLA for the surface sites we selected. Results show a relatively tightly clustered region of hydration diffusivity for BSLA when compared to results for CheY, which may be expected given our method of choosing reporter sites was to achieve comparable surface hydration behavior at each site.[71] For R1-BSLA variants, $k_{\sigma scaled}$ ranged from ~ 2-3 for all sites. Results indicate that surface waters on BSLA diffuse similarly to GroES,[56] but more slowly (*i.e.* higher $k_{\sigma scaled}$ values), on average, than that on DNA[55] or peptides of CheY[60] and the IDP IA_3 (not shown in Figure 4),[68] but less hindered (*i.e.* lower $k_{\sigma scaled}$ values) than DW on lipid bilayers or membrane proteins, which have $k_{\sigma scaled}$ values ranging up to > 6 (not shown in Figure 4).[60, 66, 75]

For R1-BSLA sites, k_{low} enhancements range from ~1.2-1.8 (defined as the ratio to k_{low} of TEMPO in water). Values of k_{low} enhancements > 1 are reflective of a population of bound water molecules.[60] The k_{low} enhancements for the R1-BSLA variants are similar to those observed for some of the 5-mer CheY peptides but higher than others[60] and on average higher than for double stranded DNA (12 bp and 24 bp),[55] and are higher than the dehydrated folding chaperone GroES [67] but lower than other sites investigated on CheY (Figure 4).

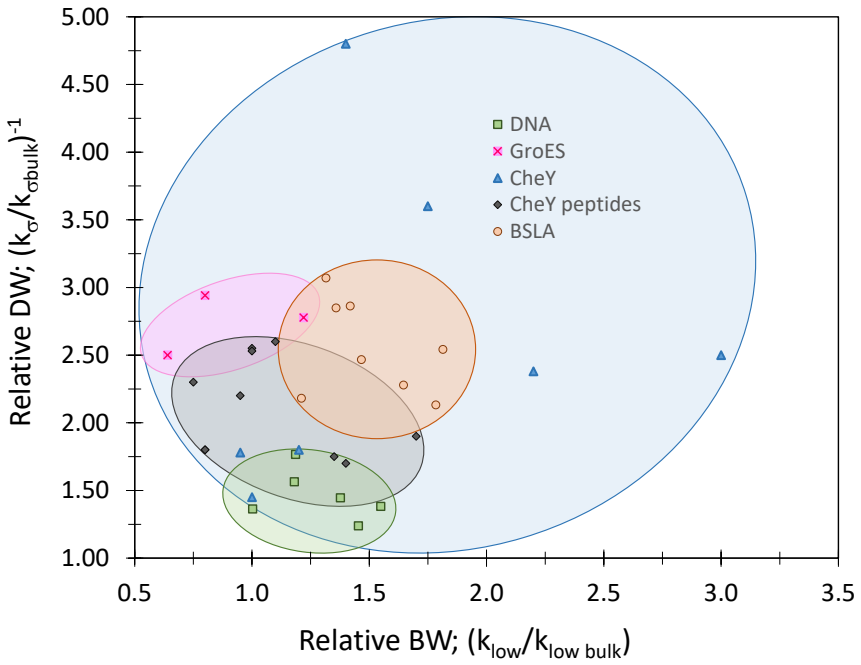

Figure 4. The BSLA phase space overlaps with that of the globular protein Chemotaxis Y, studied by Barnes *et al*.[60] and all other points in this figure were adapted from previous studies on local hydration dynamics.[55, 56, 68] Three additional sites on CheY were characterized and the data are left off this plot because they have values that extend beyond the boundaries shown.

Relating Surface Hydration Dynamics to Hydrophobic Clustering

Understanding patterns and trends in this phase space and how they relate to protein structure may help us identify the physical principles behind the changes in hydration environment from one site to another, from one variant to another, and upon addition of bioconjugates. Although the ODNP results for surface sites of R1-BSLA constructs occupy a tighter phase space than studies performed on CheY, there does appear to be some dispersion of hydration behavior. Towards elucidating the origins of the dispersion, we first evaluated if the pattern of the spread of diffusivity parameters for the R1-BSLA constructs had any relation to the secondary structure identity of each spin-labelled site. Figure 5A shows that the secondary structure identity of the spin labeled site did not directly appear to produce a straightforward pattern or trend in the phase space.

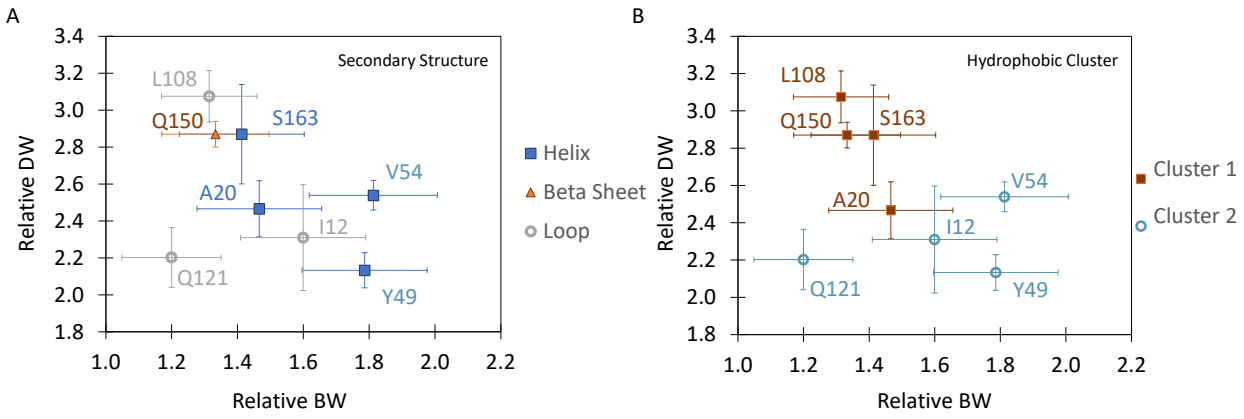

Figure 5. Relative ODNP relaxometry hydration results plotted to separate relative DW behavior (y-axis) from BW behavior (x-axis) for R1-BSLA. (A) Data points are shape and color coded according to secondary structure type. (B). Phase space of BSLA variants labeled according to the ILV cluster they reside. Error bars represent the standard deviations from three replicate measurements with errors propagated accordingly. Errors for TEMPO (bulk water) were not reported by Han and co-workers, so we estimated those values to be the average of all our errors reported in Table 1.

Recalling evolution, design and folding studies of the tryptophan synthase TIM barrel protein[38-40, 42-48] and the impact of the hydrophobic sliding mechanism on HIV-1PR,[76-82] we performed a structural ILV hydrophobic clustering of BSLA (PDB ID 1ISP). ILV clusters are domains in the protein identified by calculating close contacts of the sidechains of Isoleucine (I), Leucine (L) and Valine (V).[121] These clusters prevent the intrusion of water molecules and serve as cores of stability in globular protein structures. Using this method, the structure of BSLA was calculated to have two large (> 1000 Å^2) and two small (< 200 ILV Å^2) clusters (Table S4). The amino acid residues that comprise these groups are given in Table S5. Cluster 1 occupies ~ 2900 Å^3, contains 71 contacts with an average of 3.9 contacts/residue. Cluster 2 occupies ~ 1800 Å^3, contains 55 contacts with an average of 3.2 contacts/residue. The relative hydration phase space of DW and BW is partitioned into these two main groupings that are separated based on their location on the surface of either of the two large ILV clusters. Figure 6 shows three different views

of BSLA indicating location of the R1 incorporation and residues comprising cluster 1 and cluster 2.

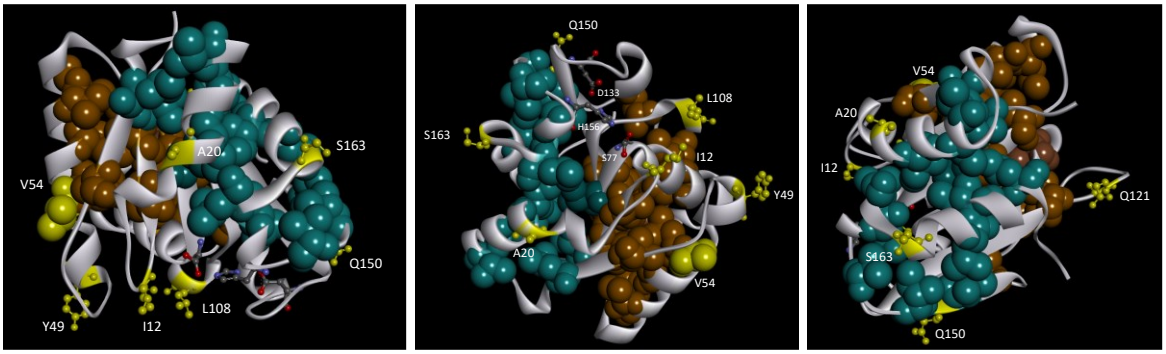

Figure 6. Ribbon diagrams depicting three different views of the hydrophobic clusters in BSLA (PDB ID 1ISP) rendered in VDW view with cluster 1 colored in dark cyan and cluster 2 colored in bronze. Sites chosen for R1 incorporation are displayed in yellow in ball and stick format. V45 is displayed in VDW and yellow indicating this chosen site occurred at a residue contained within an ILV cluster – yet still possesses surface accessibility. Active site residues S77, D133 and H156 are rendered in ball and stick format. Figures generated with Biovia Discovery Studio.

ILV analysis of the ODNP results reveals (Figure 5B) R1sites in cluster 1 (A20R1, L108R1, Q150R1, S163R1) have on average lower values of relative BW (1.38 ± 0.07 vs. 1.60 ± 0.28) and more hindered relative DW (2.82 ± .25 vs. 2.29 ± 0.17) than sites in cluster 2 (I12R1, Y49R1, V54R1). If, in this evaluation we exclude site Q121R1 in cluster 2 as it appears to be an "outlier" in its BW values compared to the other data for cluster 2, relative BW values become 1.38 ± 0.07 vs. 1.73 ± 0.10 with values of 2.82 ± .25 vs. 2.33 ± 0.20 for relative DW when comparing sites in cluster 1 to cluster 2. Additionally, in support of the hypothesis that the hydrophobic clusters influence the surface hydration properties, the relative hydration dynamics (both DW and BW) of site L108R1(cluster 1) vary significantly from those of sites I12R1 and Y49R1 (cluster 2), even though these residues reside within secondary structure elements that extend outwards from the ILV clusters and are located within close physical proximity to one another (Figure 6).

Q121R1 is located within an unstructured loop (P115-G116-T117-D118-P119-N120-Q121-K122) that extends outside of the hydrophobic cluster (Figure 6C; Figure S10) and is comprised solely of polar/charged/structure depleting amino acids, like those found in intrinsically disordered proteins (IDPs). [83-96] In fact, the relative BW behavior of Q121R1 BSLA, with value of 1.2; is on par with those of the N-terminal yeast aspartic protease inhibitor IA_3 – which we recently characterized by ODNP relaxometry,[68] having relative BW values of 1.4, which is also similar to the values obtained for the IDPs α-synuclein,[65, 66] Δtau-187[64, 67] and 5-residue peptides.[60] Accordingly, this implies that Q121R1 in BSLA, which has k_{low} enhancements ~1.4 has a sparse to no BW population. Although, our earlier computational and experimental circular dichroism studies of R1-BSLA variants showed that site Q121R had ~ 10% decrease in parallel beta sheet character and an increase in "turn" typed secondary structure, with catalytic activity ~ 80% of WT and a 3°C decrease in T_m of unfolding,[71] we view these as minor perturbations to the BSLA structure and function. We propose that the origin of the mitigated relative BW of Q121R1 in this loop region (compared to other sites in cluster 2 and cluster 1) is dictated by the high percentage of polar and charged residues of this loop; thus, resulting in relative BW hydration dynamics like those of peptides of CheY and other IDPs.

Regarding cluster 1, the relative DW behavior at site A20R1 differs from the remainder of the grouping. Although A20 is not considered within an ILV hydrophobic core, Figure 6C shows that A20 is positioned in close contact with V54 of cluster 2. Thus, perhaps the location of A20 near the interface of the two cluster domains influences the relative DW hydration behavior. In fact, relative DW values for A20R1 and V54R1 are quite similar. We further note that V54 is contained within the cluster 2 core and makes hydrophobic contact with V39 (Figure S11). Previously, our atomistic simulations indicate that V54R1 BSLA, compared to WT BSLA, may

have increased backbone fluctuations for residues 110-122 and hypothesized this observation may arise from hydrophobic sliding[76, 77, 97] communication through the ILV cluster to L114.[71] Experimentally, the V54R1 substitution in BSLA resulted in a purified enzyme that retained 90% catalytic efficiency with only a 2°C decrease in thermal stability. Again, we viewed these as minor purturbations, not significantly different from any of the other R1-BSLA constructs, so not expected to alter the DW and BW hydration behavior. Interestingly, the ODNP parameters for V54R1 and A20R1, with similar DW values but different BW values, may provide a bridge or continuum in the dispersion among values of DW and BW that impart an intermediate hydration environment that corresponds to a structural/functional association at the interface between the two hydrophobic ILV clusters.

Comparing Errors of Cross-Relaxation and Self-Relaxation Measurements.

The percentage errors in measurements of k_σ and k_ρ averaged 5-6%; because k_{low} is determined from both k_σ and k_ρ values (Eq. 9), the propagation of error increases the relative error in k_{low} to be averaged near 8% for our studies reported here. This current level of error precludes a conclusion to be drawn regarding the statistically significant separation of our data into two to three groupings as more sites on the surface of BSLA would be needed for a more thorough and valid statistical analysis. Nevertheless, the suggested pattern of separation of the hydration diffusivity of fast diffusive waters and bound water behavior correlating with hydrophobic clusters advocates for continued investigations into this potential relationship between structural fluctuations within a given hydrophobic cluster and the impacts projected onto protein surface hydration dynamics.

Conclusions

ODNP relaxometry measurements on a series of R1 spin-labeled BSLA variants reveal overall surface-like hydration diffusivity. Spin-labeled chosen for this study were previously characterized to have WT-like enzymatic behavior, secondary structure, backbone dynamics as well as thermal stability as WT-BSLA.[71] These detailed studies allowed for evaluation in understanding the origins of dispersion in DW and BW hydration parameters. Results indicate that hydrophobic core clustering location correlates with the dispersion of relative DW and BW. Hence these results set a foundation for comparison of hydration dynamics in BSLA as alterations are made to enhance thermostability, stability in organic solvents, or bioconjugation for activity in ionic liquids. Additionally, we propose that hydrophobic clustering may directly impact surface hydration through transient sampling of the unfolded conformers. Further studies will be performed to test this idea; as it seems reasonable based upon what is known about how amino acid substitutions impact the folding pathway of the tryptophan synthase TIM barrel protein.[38-40, 47, 48]

ASSOCIATED CONTENT

Supporting Information.

The Supporting Information is available free of charge at https://pubs.acs.org/doi/1.

BSLA sequences, mass spectrometry results, ODNP data analysis, ILV cluster analysis, and figures showing side-chain interactions in crystal structure as discussed within the text.

Accession Codes

BLSA (UNIPROT ID- P37957).

AUTHOR INFORMATION

Corresponding Author

Gail E Fanucci. Department of Chemistry, University of Florida, P.O. Box 117200, Gainesville, Florida 32611; Email: fanucci@chem.ufl.edu

Author Contributions

A.M.J. and A.B. designed mutagenic primers, performed PCR, confirmed sequencing, and optimized over-expression and purification of all BSLA constructs. A.M.J. performed all ODNP data collection and analysis, ILV clustering analysis and wrote the initial manuscript draft. G.E.F provided mentorship, aided in data analysis, and edited the final manuscript.

ACKNOWLEDGMENT

We thank Joel Kaar, Department of Chemical and Biochemical Engineering, University of Colorado, for helpful discussions regarding protein purification and optimization of sample homogeneity at concentrations required for magnetic resonance studies. We thank Coray M Colina, Department of Chemistry, University of Florida, for helpful discussions and co-mentoring of A.M.J. in computational aspects of Lipase A. We acknowledge the UF Provost office in support of the CURE program.

Funding Sources

This study was supported by NSF (MCB-1715384 and CHE-2003366; GEF), NIH (S10 RR031603; GEF) NIH S10 OD021758-01A1 (UF Chemistry Mass Spectrometry Facility).

ABBREVIATIONS

BSLA, *Bacillus subtilis* Lipase A; ODNP, Overhauser DNP; DW, diffusive water; BW, bound water; ILV; isoleucine leucine and valine.

REFERENCES

(1) Akram, F.; Mir, A. S.; Haq, I. U.; Roohi, A., An Appraisal on Prominent Industrial and Biotechnological Applications of Bacterial Lipases. *Mol. Biotechnol.* **2023,** *65*, 521-543.
(2) Anobom, C. D.; Pinheiro, A. S.; De-Andrade, R. A.; Aguieiras, E. C.; Andrade, G. C.; Moura, M. V.; Almeida, R. V.; Freire, D. M., From Structure to Catalysis: Recent Developments in the Biotechnological Applications of Lipases. *Biomed. Res. Int.* **2014,** *2014*, 684506.
(3) Ismail, A. R.; Baek, K. H., Lipase Immobilization with Support Materials, Preparation Techniques, and Applications: Present and Future Aspects. *Int. J. Biol. Macromol.* **2020,** *163*, 1624-1639.
(4) Chandra, P.; Enespa; Singh, R.; Arora, P. K., Microbial Lipases and Their Industrial Applications: A Comprehensive Review. *Microb. Cell. Fact.* **2020,** *19*, 169.
(5) Mahfoudhi, A.; Benmabrouk, S.; Fendri, A.; Sayari, A., Fungal Lipases as Biocatalysts: A Promising Platform in Several Industrial Biotechnology Applications. *Biotechnol. Bioeng.* **2022,** *119*, 3370-3392.
(6) Ali, S.; Khan, S. A.; Hamayun, M.; Lee, I. J., The Recent Advances in the Utility of Microbial Lipases: A Review. *Microorganisms* **2023,** *11*.
(7) Kumar, A.; Verma, V.; Dubey, V. K.; Srivastava, A.; Garg, S. K.; Singh, V. P.; Arora, P. K., Industrial Applications of Fungal Lipases: A Review. *Front. Microbiol.* **2023,** *14*, 1142536.
(8) Kennedy, M. B.; Lennarz, W. J., Characterization of the Extracellular Lipase of Bacillus Subtilis and Its Relationship to a Membrane-Bound Lipase Found in a Mutant Strain. *J. Biol. Chem.* **1979,** *254*, 1080-9.
(9) Dartois, V.; Baulard, A.; Schanck, K.; Colson, C., Cloning, Nucleotide Sequence and Expression in Escherichia Coli of a Lipase Gene from Bacillus Subtilis 168. *Biochim. Biophys. Acta* **1992,** *1131*, 253-60.
(10) Lesuisse, E.; Schanck, K.; Colson, C., Purification and Preliminary Characterization of the Extracellular Lipase of Bacillus Subtilis 168, an Extremely Basic Ph-Tolerant Enzyme. *Eur. J. Biochem.* **1993,** *216*, 155-60.
(11) Khan, F. I.; Lan, D.; Durrani, R.; Huan, W.; Zhao, Z.; Wang, Y., The Lid Domain in Lipases: Structural and Functional Determinant of Enzymatic Properties. *Front. Bioeng. Biotechnol.* **2017,** *5*, 16.
(12) van Pouderoyen, G.; Eggert, T.; Jaeger, K. E.; Dijkstra, B. W., The Crystal Structure of Bacillus Subtilis Lipase: A Minimal Alpha/Beta Hydrolase Fold Enzyme. *J. Mol. Bio.l* **2001,** *309*, 215-26.
(13) Das, S.; Behera, S.; Balasubramanian, S., Orientational Switch of the Lipase a Enzyme at the Oil-Water Interface: An Order of Magnitude Increase in Turnover Rate with a Single Surfactant Tag Explained. *J. Phys. Chem. Lett.* **2020,** *11*, 2977-2982.

(14) Behera, S.; Balasubramanian, S., Lipase a from Bacillus Subtilis: Substrate Binding, Conformational Dynamics, and Signatures of a Lid. *J. Chem. Inf. Model.* **2023,** *63*, 7545-7556.
(15) Belle, V.; Fournel, A.; Woudstra, M.; Ranaldi, S.; Prieri, F.; Thome, V.; Currault, J.; Verger, R.; Guigliarelli, B.; Carriere, F., Probing the Opening of the Pancreatic Lipase Lid Using Site-Directed Spin Labeling and Epr Spectroscopy. *Biochemistry* **2007,** *46*, 2205-14.
(16) Brocca, S.; Secundo, F.; Ossola, M.; Alberghina, L.; Carrea, G.; Lotti, M., Sequence of the Lid Affects Activity and Specificity of Candida Rugosa Lipase Isoenzymes. *Protein. Sci.* **2003,** *12*, 2312-9.
(17) Ahmad, S.; Kamal, M. Z.; Sankaranarayanan, R.; Rao, N. M., Thermostable Bacillus Subtilis Lipases: In Vitro Evolution and Structural Insight. *J. Mol. Biol.* **2008,** *381*, 324-40.
(18) Augustyniak, W.; Brzezinska, A. A.; Pijning, T.; Wienk, H.; Boelens, R.; Dijkstra, B. W.; Reetz, M. T., Biophysical Characterization of Mutants of Bacillus Subtilis Lipase Evolved for Thermostability: Factors Contributing to Increased Activity Retention. *Protein. Sci.* **2012,** *21*, 487-97.
(19) Augustyniak, W.; Wienk, H.; Boelens, R.; Reetz, M. T., (1)H, (1)(3)C and (1)(5)N Resonance Assignments of Wild-Type Bacillus Subtilis Lipase a and Its Mutant Evolved Towards Thermostability. *Biomol. NMR Assign.* **2013,** *7*, 249-52.
(20) Kamal, M. Z.; Ahmad, S.; Molugu, T. R.; Vijayalakshmi, A.; Deshmukh, M. V.; Sankaranarayanan, R.; Rao, N. M., In Vitro Evolved Non-Aggregating and Thermostable Lipase: Structural and Thermodynamic Investigation. *J. Mol. Bio.l* **2011,** *413*, 726-41.
(21) Kamal, M. Z.; Ahmad, S.; Yedavalli, P.; Rao, N. M., Stability Curves of Laboratory Evolved Thermostable Mutants of a Bacillus Subtilis Lipase. *Biochim. Biophys. Acta* **2010,** *1804*, 1850-6.
(22) Kamal, M. Z.; Mohammad, T. A.; Krishnamoorthy, G.; Rao, N. M., Role of Active Site Rigidity in Activity: Md Simulation and Fluorescence Study on a Lipase Mutant. *PLoS One* **2012,** *7*, e35188.
(23) Kumar, R.; Goomber, S.; Kaur, J., Engineering Lipases for Temperature Adaptation: Structure Function Correlation. *Biochim. Biophys. Acta Proteins Proteom.* **2019,** *1867*, 140261.
(24) Zhao, J.; Frauenkron-Machedjou, V. J.; Fulton, A.; Zhu, L.; Davari, M. D.; Jaeger, K. E.; Schwaneberg, U.; Bocola, M., Unraveling the Effects of Amino Acid Substitutions Enhancing Lipase Resistance to an Ionic Liquid: A Molecular Dynamics Study. *Phys. Chem. Chem. Phys.* **2018,** *20*, 9600-9609.
(25) Burney, P. R.; Nordwald, E. M.; Hickman, K.; Kaar, J. L.; Pfaendtner, J., Molecular Dynamics Investigation of the Ionic Liquid/Enzyme Interface: Application to Engineering Enzyme Surface Charge. *Proteins* **2015,** *83*, 670-80.
(26) Martinez, R.; Bernal, C.; Alvarez, R.; Concha, C.; Araya, F.; Cabrera, R.; Dhoke, G. V.; Davari, M. D., Deletion and Randomization of Structurally Variable Regions in B. Subtilis Lipase a (Bsla) Alter Its Stability and Hydrolytic Performance against Long Chain Fatty Acid Esters. *Int. J. Mol. Sci.* **2020,** 14;*21*(6) :1990. doi: 10.3390/ijms21061990. PMID: 32183336; PMCID: PMC7139672
(27) Funke, S. A.; Eipper, A.; Reetz, M. T.; Otte, N.; Thiel, W.; Van Pouderoyen, G.; Dijkstra, B. W.; Jaeger, K. E.; Eggert, T., Directed Evolution of an Enantioselective Bacillus Subtilis Lipase. *Biocatal. Biotransformation* **2003,** *21*, 67-73.
(28) Lyu, J.; Li, Z.; J., M.; Jiang, R.; Tang, G.; Zhou, Y.; Gao, R., Covalent Immobilization of Bacillus Subtilis Lipase a on Fe3o4 Nanoparticles by Aldehyde Tag: An Ideal Immobilization with Minimal Chemical Modification. *Process Biochemistry* **2019,** *81*, 63-69.

(29) Nordwald, E. M.; Armstrong, G. S.; Kaar, J. L., Nmr-Guided Rational Engineering of an Ionic-Liquid-Tolerant Lipase. *ACS Catal.* **2014,** *4*, 4057-4064.
(30) Cui, H.; Vedder, M.; Zhang, L.; Jaeger, K. E.; Schwaneberg, U.; Davari, M. D., Polar Substitutions on the Surface of a Lipase Substantially Improve Tolerance in Organic Solvents. *Chem.Sus.Chem.* **2022,** *15*, e202102551.
(31) Zhang, L.; Ding, Y., The Relation between Lipase Thermostability and Dynamics of Hydrogen Bond and Hydrogen Bond Network Based on Long Time Molecular Dynamics Simulation. *Protein Pept. Lett.* **2017,** *24*, 643-648.
(32) Klahn, M.; Lim, G. S.; Wu, P., How Ion Properties Determine the Stability of a Lipase Enzyme in Ionic Liquids: A Molecular Dynamics Study. *Phys. Chem. Chem. Phys.* **2011,** *13*, 18647-60.
(33) Cui, H.; Eltoukhy, L.; Zhang, L.; Markel, U.; Jaeger, K. E.; Davari, M. D.; Schwaneberg, U., Less Unfavorable Salt Bridges on the Enzyme Surface Result in More Organic Cosolvent Resistance. *Angew. Chem. Int. Ed. Engl.* **2021,** *60*, 11448-11456.
(34) Zhou, Y.; Jones, N. C.; Nedergaard Pedersen, J.; Perez, B.; Vronning Hoffmann, S.; Vang Petersen, S.; Skov Pedersen, J.; Perriman, A.; Kristensen, P.; Gao, R.; Guo, Z., Insight into the Structure and Activity of Surface-Engineered Lipase Biofluids. *Chembiochem* **2019,** *20*, 1266-1272.
(35) Chado, G. R.; Holland, E. N.; Tice, A. K.; Stoykovich, M. P.; Kaar, J. L., Modification of Lipase with Poly(4-Acryloylmorpholine) Enhances Solubility and Transesterification Activity in Anhydrous Ionic Liquids. *Biomacromolecules* **2018,** *19*, 1324-1332.
(36) Behera, S.; Balasubramanian, S., Insights into Substrate Behavior in a Solvent-Free Protein Liquid to Rationalize Its Reduced Catalytic Rate. *RSC Adv* **2022,** *12*, 11896-11905.
(37) Zhou, Y.; Pedersen, J. N.; Pedersen, J. N.; Jones, N. C.; Hoffmann, S. V.; Petersen, S. V.; Pedersen, J. S.; Perriman, A.; Gao, R.; Guo, Z., Superanionic Solvent-Free Liquid Enzymes Exhibit Enhanced Structures and Activities. *Adv. Sci. (Weinh)* **2022,** *9*, e2202359.
(38) Vadrevu, R.; Wu, Y.; Matthews, C. R., Nmr Analysis of Partially Folded States and Persistent Structure in the Alpha Subunit of Tryptophan Synthase: Implications for the Equilibrium Folding Mechanism of a 29-Kda Tim Barrel Protein. *J. Mol. Biol.* **2008,** *377*, 294-306.
(39) Wu, Y.; Vadrevu, R.; Kathuria, S.; Yang, X.; Matthews, C. R., A Tightly Packed Hydrophobic Cluster Directs the Formation of an Off-Pathway Sub-Millisecond Folding Intermediate in the Alpha Subunit of Tryptophan Synthase, a Tim Barrel Protein. *J. Mol. Biol.* **2007,** *366*, 1624-38.
(40) Yang, X.; Vadrevu, R.; Wu, Y.; Matthews, C. R., Long-Range Side-Chain-Main-Chain Interactions Play Crucial Roles in Stabilizing the (Betaalpha)8 Barrel Motif of the Alpha Subunit of Tryptophan Synthase. *Protein Sci.* **2007,** *16*, 1398-409.
(41) Basak, S.; Nobrega, R. P.; Tavella, D.; Deveau, L. M.; Koga, N.; Tatsumi-Koga, R.; Baker, D.; Massi, F.; Matthews, C. R., Networks of Electrostatic and Hydrophobic Interactions Modulate the Complex Folding Free Energy Surface of a Designed Betaalpha Protein. *Proc. Natl. Acad. Sci. U S A* **2019,** *116*, 6806-6811.
(42) Kordes, S.; Beck, J.; Shanmugaratnam, S.; Flecks, M.; Hocker, B., Physics-Based Approach to Extend a De Novo Tim Barrel with Rationally Designed Helix-Loop-Helix Motifs. *Protein Eng. Des. Sel.* **2023,** *36*, gzad012. https://doi.org/10.1093/protein/gzad012

(43) Kordes, S.; Romero-Romero, S.; Lutz, L.; Hocker, B., A Newly Introduced Salt Bridge Cluster Improves Structural and Biophysical Properties of De Novo Tim Barrels. *Protein Sci.* **2022,** *31*, 513-527.
(44) Wiese, J. G.; Shanmugaratnam, S.; Hocker, B., Extension of a De Novo Tim Barrel with a Rationally Designed Secondary Structure Element. *Protein Sci.* **2021,** *30*, 982-989.
(45) Romero-Romero, S.; Kordes, S.; Michel, F.; Hocker, B., Evolution, Folding, and Design of Tim Barrels and Related Proteins. *Curr. Opin. Struct. Biol.* **2021,** *68*, 94-104.
(46) Romero-Romero, S.; Costas, M.; Silva Manzano, D. A.; Kordes, S.; Rojas-Ortega, E.; Tapia, C.; Guerra, Y.; Shanmugaratnam, S.; Rodriguez-Romero, A.; Baker, D.; Hocker, B.; Fernandez-Velasco, D. A., The Stability Landscape of De Novo Tim Barrels Explored by a Modular Design Approach. *J. Mol. Biol.* **2021,** *433*, 167153.
(47) Jain, R.; Muneeruddin, K.; Anderson, J.; Harms, M. J.; Shaffer, S. A.; Matthews, C. R., A Conserved Folding Nucleus Sculpts the Free Energy Landscape of Bacterial and Archaeal Orthologs from a Divergent Tim Barrel Family. *Proc. Natl. Acad. Sci. U S A* **2021,** *118*.
(48) Chan, Y. H.; Zeldovich, K. B.; Matthews, C. R., An Allosteric Pathway Explains Beneficial Fitness in Yeast for Long-Range Mutations in an Essential Tim Barrel Enzyme. *Protein Sci.* **2020,** *29*, 1911-1923.
(49) Franck, J. M.; Han, S., Overhauser Dynamic Nuclear Polarization for the Study of Hydration Dynamics, Explained. *Methods Enzymol.* **2019,** *615*, 131-175.
(50) Franck, J. M.; Pavlova, A.; Scott, J. A.; Han, S., Quantitative Cw Overhauser Effect Dynamic Nuclear Polarization for the Analysis of Local Water Dynamics. *Prog. Nucl. Magn. Reson. Spectrosc.* **2013,** *74*, 33-56.
(51) Doll, A.; Bordignon, E.; Joseph, B.; Tschaggelar, R.; Jeschke, G., Liquid State Dnp for Water Accessibility Measurements on Spin-Labeled Membrane Proteins at Physiological Temperatures. *J. Magn. Reson.* **2012,** *222*, 34-43.
(52) Overhauser, A. W., Polarization of Nuclei in Metals. *Phys Rev* **1953,** *91*, 476-476.
(53) Hausser, K. H.; Stehlik, D., Dynamic Nuclear Polarization in Liquids. *Advances in Magnetic and Optical Resonance* **1968,** *3*, 79-139.
(54) Hwang, L. P.; Freed, J. H., Dynamic Effects of Pair Correlation-Functions on Spin Relaxation by Translational Diffusion in Liquids. *J. Chem. Phys.* **1975,** *63*, 4017-4025.
(55) Franck, J. M.; Ding, Y.; Stone, K.; Qin, P. Z.; Han, S., Anomalously Rapid Hydration Water Diffusion Dynamics near DNA Surfaces. *J. Am. Chem. Soc.* **2015,** *137*, 12013-23.
(56) Franck, J. M.; Sokolovski, M.; Kessler, N.; Matalon, E.; Gordon-Grossman, M.; Han, S. I.; Goldfarb, D.; Horovitz, A., Probing Water Density and Dynamics in the Chaperonin Groel Cavity. *J. Am. Chem. Soc.* **2014,** *136*, 9396-403.
(57) Armstrong, B. D.; Choi, J.; Lopez, C.; Wesener, D. A.; Hubbell, W.; Cavagnero, S.; Han, S., Site-Specific Hydration Dynamics in the Nonpolar Core of a Molten Globule by Dynamic Nuclear Polarization of Water. *J. Am. Chem. Soc.* **2011,** *133*, 5987-95.
(58) Armstrong, B. D.; Han, S., Overhauser Dynamic Nuclear Polarization to Study Local Water Dynamics. *J. Am. Chem. Soc.* **2009,** *131*, 4641-7.
(59) Kaminker, I.; Barnes, R.; Han, S., Overhauser Dynamic Nuclear Polarization Studies on Local Water Dynamics. *Methods Enzymol.* **2015,** *564*, 457-83.
(60) Barnes, R.; Sun, S.; Fichou, Y.; Dahlquist, F. W.; Heyden, M.; Han, S., Spatially Heterogeneous Surface Water Diffusivity around Structured Protein Surfaces at Equilibrium. *J. Am. Chem. Soc.* **2017,** *139*, 17890-17901.

(61) Kausik, R.; Srivastava, A.; Korevaar, P. A.; Stucky, G.; Waite, J. H.; Han, S., Local Water Dynamics in Coacervated Polyelectrolytes Monitored through Dynamic Nuclear Polarization-Enhanced H Nmr. *Macromolecules* **2009,** *42*, 7404-7412.
(62) Cheng, C. Y.; Wang, J. Y.; Kausik, R.; Lee, K. Y.; Han, S., An Ultrasensitive Tool Exploiting Hydration Dynamics to Decipher Weak Lipid Membrane-Polymer Interactions. *J. Magn. Reson.* **2012,** *215*, 115-9.
(63) Ortony, J. H.; Cheng, C.-Y.; Franck, J. M.; Kausik, R.; Pavlova, A.; Hunt, J.; Han, S., Probing the Hydration Water Diffusion of Macromolecular Surfaces and Interfaces. *New Journal of Physics* **2011,** *13*.
(64) Pavlova, A.; McCarney, E. R.; Peterson, D. W.; Dahlquist, F. W.; Lew, J.; Han, S., Site-Specific Dynamic Nuclear Polarization of Hydration Water as a Generally Applicable Approach to Monitor Protein Aggregation. *Phys. Chem. Chem. Phys.* **2009,** *11*, 6553-4.
(65) Cheng, C. Y.; Varkey, J.; Ambroso, M. R.; Langen, R.; Han, S., Hydration Dynamics as an Intrinsic Ruler for Refining Protein Structure at Lipid Membrane Interfaces. *Proc. Natl. Acad .Sci. U S A* **2013,** *110*, 16838-43.
(66) Fisette, O.; Paslack, C.; Barnes, R.; Isas, J. M.; Langen, R.; Heyden, M.; Han, S.; Schafer, L. V., Hydration Dynamics of a Peripheral Membrane Protein. *J. Am. Chem. Soc.* **2016,** *138*, 11526-35.
(67) Pavlova, A.; Cheng, C. Y.; Kinnebrew, M.; Lew, J.; Dahlquist, F. W.; Han, S., Protein Structural and Surface Water Rearrangement Constitute Major Events in the Earliest Aggregation Stages of Tau. *Proc. Nat.l Acad. Sci. U S A* **2016,** *113*, E127-36.
(68) Dunleavy, K. M.; Li, T.; Milshteyn, E.; Jaufer, A. M.; Walker, S. A.; Fanucci, G. E., Charge Distribution Patterns of IA_3 Impact Conformational Expansion and Hydration Diffusivity of the Disordered Ensemble. *J. Phys. Chem. B* **2023,** *127*, 9734-9746.
(69) Kausik, R.; Han, S., Dynamics and State of Lipid Bilayer-Internal Water Unraveled with Solution State 1h Dynamic Nuclear Polarization. *Phys. Chem. Chem. Phys.* **2011,** *13*, 7732-46.
(70) Nthangeni, M. B.; Patterton, H.; van Tonder, A.; Vergeer, W. P.; Litthauer, D., Over-Expression and Properties of a Purified Recombinant Bacillus Licheniformis Lipase: A Comparative Report on Bacillus Lipases. *Enzyme Microb. Technol.* **2001,** *28*, 705-712.
(71) Jaufer, A. M.; Bouhadana, A.; Kharrazizadeh, A.; Zhou, M.; Colina, C. M.; Fanucci, G. E., Designing Surface Exposed Sites on Bacillus Subtilis Lipase a for Spin-Labeling and Hydration Studies. *Biophys. Chem.* **2024,** *308*, 107203.
(72) Kawasaki, K.; Kondo, H.; Suzuki, M.; Ohgiya, S.; Tsuda, S., Alternate Conformations Observed in Catalytic Serine of Bacillus Subtilis Lipase Determined at 1.3 a Resolution. *Acta Crystallogr. D Bio.l Crystallogr.* **2002,** *58*, 1168-74.
(73) Armstrong, B. D.; Lingwood, M.; McCarney, E.; Brown, E. R.; Blümler, P.; Han, S., Portable X-Band System for Solution State Dynamic Nuclear Polarization. *J. Magn. Reson.* **2008,** *191*, 273-281.
(74) Moon, H.; Collanton, R. P.; Monroe, J. I.; Casey, T. M.; Shell, M. S.; Han, S.; Scott, S. L., Evidence for Entropically Controlled Interfacial Hydration in Mesoporous Organosilicas. *J. Am. Chem. Soc.* **2022,** *144*, 1766-1777.
(75) Hong, Y.; Najafi, S.; Casey, T.; Shea, J. E.; Han, S. I.; Hwang, D. S., Hydrophobicity of Arginine Leads to Reentrant Liquid-Liquid Phase Separation Behaviors of Arginine-Rich Proteins. *Nat. Commun.* **2022,** *13*, 7326.

(76) Sherry, D.; Pandian, R.; Sayed, Y., Non-Active Site Mutations in the Hiv Protease: Diminished Drug Binding Affinity Is Achieved through Modulating the Hydrophobic Sliding Mechanism. *Int. J. Biol. Macromol.* **2022,** *217*, 27-41.
(77) Foulkes-Murzycki, J. E.; Scott, W. R.; Schiffer, C. A., Hydrophobic Sliding: A Possible Mechanism for Drug Resistance in Human Immunodeficiency Virus Type 1 Protease. *Structure* **2007,** *15*, 225-33.
(78) Tran, T. T.; Liu, Z.; Fanucci, G. E., Conformational Landscape of Non-B Variants of Hiv-1 Protease: A Pulsed Epr Study. *Biochem. Biophys. Res. Commun.* **2020,** *532*, 219-224.
(79) Liu, Z.; Tran, T. T.; Pham, L.; Hu, L.; Bentz, K.; Savin, D. A.; Fanucci, G. E., Darunavir-Resistant Hiv-1 Protease Constructs Uphold a Conformational Selection Hypothesis for Drug Resistance. *Viruses* **2020,** *12*.
(80) de Vera, I. M.; Smith, A. N.; Dancel, M. C.; Huang, X.; Dunn, B. M.; Fanucci, G. E., Elucidating a Relationship between Conformational Sampling and Drug Resistance in Hiv-1 Protease. *Biochemistry* **2013,** *52*, 3278-88.
(81) de Vera, I. M.; Blackburn, M. E.; Fanucci, G. E., Correlating Conformational Shift Induction with Altered Inhibitor Potency in a Multidrug Resistant Hiv-1 Protease Variant. *Biochemistry* **2012,** *51*, 7813-5.
(82) Carter, J. D.; Gonzales, E. G.; Huang, X.; Smith, A. N.; de Vera, I. M.; D'Amore, P. W.; Rocca, J. R.; Goodenow, M. M.; Dunn, B. M.; Fanucci, G. E., Effects of Pre and Post Therapy Drug-Pressure Selected Mutations on Hiv-1 Protease Conformational Sampling. *FEBS Lett* **2014,** *588*, 3123-8.
(83) Das, R. K.; Pappu, R. V., Conformations of Intrinsically Disordered Proteins Are Influenced by Linear Sequence Distributions of Oppositely Charged Residues. *Proc. Natl. Acad. Sci. U S A* **2013,** *110*, 13392-7.
(84) Tompa, P., Intrinsically Unstructured Proteins. *TRENDS in Biochemical Sciences* **2002,** *27*, 527-533.
(85) Dunker, A. K.; Oldfield, C. J.; Meng, J.; Romero, P.; Yang, J. Y.; Chen, J. W.; Vacic, V.; Obradovic, Z.; Uversky, V. N., The Unfoldomics Decade: An Update on Intrinsically Disordered Proteins. *BMC Genomics* **2008,** *9 Suppl 2*, S1.
(86) Habchi, J.; Tompa, P.; Longhi, S.; Uversky, V. N., Introducing Protein Intrinsic Disorder. *Chem. Rev* **2014,** *114*, 6561-88.
(87) Vihinen, M.; Torkkila, E.; Riikonen, P., Accuracy of Protein Flexibility Predictions. *Proteins* **1994,** *19*, 141-9.
(88) Marsh, J. A.; Forman-Kay, J. D., Sequence Determinants of Compaction in Intrinsically Disordered Proteins. *Biophys. J.* **2010,** *98*, 2383-90.
(89) Mao, A. H.; Crick, S. L.; Vitalis, A.; Chicoine, C. L.; Pappu, R. V., Net Charge Per Residue Modulates Conformational Ensembles of Intrinsically Disordered Proteins. *Proc. Natl. Acad. Sci. U S A* **2010,** *107*, 8183-8.
(90) Holehouse, A. S.; Das, R. K.; Ahad, J. N.; Richardson, M. O.; Pappu, R. V., Cider: Resources to Analyze Sequence-Ensemble Relationships of Intrinsically Disordered Proteins. *Biophys. J.* **2017,** *112*, 16-21.
(91) Das, R. K.; Ruff, K. M.; Pappu, R. V., Relating Sequence Encoded Information to Form and Function of Intrinsically Disordered Proteins. *Curr. Opin. Struct. Biol.* **2015,** *32*, 102-12.
(92) Baul, U.; Chakraborty, D.; Mugnai, M. L.; Straub, J. E.; Thirumalai, D., Sequence Effects on Size, Shape, and Structural Heterogeneity in Intrinsically Disordered Proteins. *J. Phys. Chem. B* **2019,** *123*, 3462-3474.

(93) Bianchi, G.; Longhi, S.; Grandori, R.; Brocca, S., Relevance of Electrostatic Charges in Compactness, Aggregation, and Phase Separation of Intrinsically Disordered Proteins. *Int. J. Mol. Sci.* **2020,** *21*, 6208.
(94) Brocca, S.; Grandori, R.; Longhi, S.; Uversky, V., Liquid-Liquid Phase Separation by Intrinsically Disordered Protein Regions of Viruses: Roles in Viral Life Cycle and Control of Virus-Host Interactions. *Int. J. Mol. Sci.* **2020,** *21*, 9045.
(95) Uversky, V. N.; Gillespie, J. R.; Fink, A. L., Why Are "Natively Unfolded" Proteins Unstructured under Physiologic Conditions? *Proteins* **2000,** *41*, 415-27.
(96) Muller-Spath, S.; Soranno, A.; Hirschfeld, V.; Hofmann, H.; Ruegger, S.; Reymond, L.; Nettels, D.; Schuler, B., From the Cover: Charge Interactions Can Dominate the Dimensions of Intrinsically Disordered Proteins. *Proc. Natl. Acad. Sci. U S A* **2010,** *107*, 14609-14.
(97) Wong, K.; Geiduschek, E. P., Activator-Sigma Interaction: A Hydrophobic Segment Mediates the Interaction of a Sigma Family Promoter Recognition Protein with a Sliding Clamp Transcription Activator. *J. Mol. Biol.* **1998,** *284*, 195-203.